Am J Physiol Regul Integr Comp Physiol 291: R1688–R1699, 2006.
First published July 13, 2006; doi:10.1152/ajpregu.00261.2006.

Descending vasa recta endothelium is an electrical syncytium

Qingli Zhang,[1] Chunhua Cao,[1] Michael Mangano,[3] Zhong Zhang,[1] Erik P. Silldorff,[3] Whaseon Lee-Kwon,[1] Kristie Payne,[1] and Thomas L. Pallone[1,2]

[1]*Division of Nephrology, Department of Medicine, and* [2]*Department of Physiology, University of Maryland School of Medicine, Baltimore; and* [3]*Department of Biology, Towson University, Towson, Maryland*

Submitted 17 April 2006; accepted in final form 7 July 2006

Zhang, Qingli, Chunhua Cao, Michael Mangano, Zhong Zhang, Erik P. Silldorff, Whaseon Lee-Kwon, Kristie Payne, and Thomas L. Pallone. Descending vasa recta endothelium is an electrical syncytium. *Am J Physiol Regul Integr Comp Physiol* 291: R1688–R1699, 2006. First published July 13, 2006; doi:10.1152/ajpregu.00261.2006.—We examined gap junction coupling of descending vasa recta (DVR). DVR endothelial cells or pericytes were depolarized to record the associated capacitance transients. Virtually all endothelia and some pericytes exhibited prolonged transients lasting 10–30 ms. Carbenoxolone (100 μM) and 18β-glycyrrhetinic acid (18βGRA; 100 μM) markedly shortened the endothelial transients. Carbenoxolone and heptanol (2 mM) reduced the pericyte capacitance transients when they were prolonged. Lucifer yellow (LY; 2 mM) was dialyzed into the cytoplasm of endothelial cells and pericytes. LY spread diffusely along the endothelial monolayer, whereas in most pericytes, it was confined to a single cell. In some pericytes, complex patterns of LY spreading were observed. DVR cells were depolarized by voltage clamp as fluorescence of bis(1,3-dibarbituric acid)-trimethine oxanol [$DiBAC_4(3)$] was monitored ~200 μm away. A 40-mV endothelial depolarization was accompanied by a 26.1 ± 5.5-mV change in $DiBAC_4(3)$ fluorescence. $DiBAC_4(3)$ fluorescence did not change after 18βGRA or when pericytes were depolarized. Similarly, propagated cytoplasmic Ca^{2+} responses arising from mechanical perturbation of the DVR wall were attenuated by 18βGRA or heptanol. Connexin (Cx) immunostaining showed predominant linear Cx40 and Cx43 in endothelia, whereas Cx37 stained smooth muscle actin-positive pericytes. We conclude that the DVR endothelium is an electrical syncytium and that gap junction coupling in DVR pericytes exists but is less pronounced.

rat; kidney; medulla; microcirculation; electrophysiology; blood flow

DESCENDING VASA RECTA (DVR) are ~12- to 18-μm-diameter branches of juxtamedullary efferent arterioles that supply the renal medulla with blood flow. In addition to their role in countercurrent exchange (39), they are surrounded by smooth muscle-like cells (pericytes) that contract and dilate in response to a variety of hormonal and paracrine agents (38, 40). In an ongoing effort to delineate the channel architecture of DVR, we devised methods to patch clamp either the abluminal pericytes or luminal endothelia of explanted vessels (44). Those approaches have been used to define the regulation of membrane potential (37, 59), K^+ currents (5), and cation entry pathways (55, 59). As previously described, prolonged, decaying capacitance transients, possibly attributable to cell-to-cell coupling through gap junctions, are sometimes observed upon patch clamp of pericytes of intact explanted vessels. When the goal of the experiment has been to measure single-cell ion currents, study of such cells was abandoned. Similar prolonged capacitance transients are nearly always found when electrical access to DVR endothelial cells has been obtained using whole cell patch-clamp methods (5, 44, 55).

In this study, we tested whether those prolonged transients arise from gap junction coupling in the DVR wall. In both pericytes and endothelium, application of gap junction blockers reduced the time of decay time of the transients from 10 to 30 ms to <1 ms. The fluorescent probe Lucifer yellow (457 Da) was found to diffuse freely from cell to cell in the endothelial monolayer. In contrast, Lucifer yellow was most often sequestered within single pericytes. Depolarizing pulses imposed by voltage clamp were readily conducted along the endothelial monolayer. Similar electrical spreading was not observed from patched pericytes. Cytoplasmic Ca^{2+} responses ($[Ca^{2+}]_{cyt}$) that propagated away from a point of mechanical stimulation of the DVR wall were attenuated by gap junction blockade. Finally, immunochemical staining showed predominant expression of connexin (Cx)40 and Cx43 in the endothelium and predominantly Cx37 in pericytes. We conclude that the DVR endothelium is an electrical syncytium. In contrast, open gap junctions between adjacent pericytes or between pericytes and the underlying endothelium exist but are less common.

METHODS

Isolation of DVR. Investigations involving animal use were performed according to protocols approved by the Institutional Animal Care and Use Committee of the University of Maryland. Kidneys were harvested from Sprague-Dawley rats (120–200 g; Harlan) that had been anesthetized with an intraperitoneal injection of ketamine (80 mg/kg)-xylazine (10 mg/kg). Tissue slices were stored at 4°C in a physiological saline solution (PSS). For patch clamp of pericytes, wedges of renal medulla were enzymatically digested in Blendzyme 1 (0.27 mg/ml; Roche) in high-glucose DMEM medium (Invitrogen) at 37°C for 45 min. Access to endothelial cells for patch clamp necessitated removal of pericytes from the abluminal surface. This was done, as previously described in detail (44), by drawing the vessel into the mouth of a micropipette that had been heat-polished to ~6 μm. For those protocols, tissue digestion was performed in a cocktail of collagenase 1A (0.5 mg/ml), protease XIV (0.4 mg/ml), and bovine serum albumin (1.0 mg/ml) in PSS (in mM: 155 NaCl, 5 KCl, 1 $MgCl_2$, 1 $CaCl_2$, 10 HEPES, and 10 glucose, pH 7.4). In all cases, after digestion, medullary tissue was transferred to PSS and held at 4°C. DVR were isolated by microdissection as needed and transferred to an inverted microscope (Nikon TE300) for patch-clamp recording and fluorescent microscopy.

Whole cell patch-clamp recording. Patch pipettes were made from borosilicate glass (PG52151-4, external diameter 1.5 mm, internal diameter 1.0 mm; World Precision Instruments, Sarasota, FL) with the

Address for reprint requests and other correspondence: T. L. Pallone, Division of Nephrology, N3W143, 22 S. Greene St., UMMS, Baltimore, MD 21201 (e-mail: tpallone@medicine.umaryland.edu).

The costs of publication of this article were defrayed in part by the payment of page charges. The article must therefore be hereby marked "*advertisement*" in accordance with 18 U.S.C. Section 1734 solely to indicate this fact.

use of a two-stage vertical pipette puller (Narshige PP-830) and were heat-polished. Whole cell currents were recorded using either the nystatin-perforated patch or ruptured patch configurations as previously described (5, 37, 55). For nystatin-perforated patches or ruptured patches used to dialyze Lucifer yellow into the cell cytoplasm, the electrode solution contained (in mM) 120 K-aspartate, 20 KCl, 10 NaCl, and 10 HEPES, pH 7.2, and nystatin (100 μg/ml with 0.1% DMSO) in ultrapure water. For protocols that focused on measurement of membrane capacitance, membrane currents were minimized with the following electrode solution (in mM): 115 Cs-methanesulfonate, 18 CsCl, 10 NaCl, 2.35 MgATP, 1 $CaCl_2$, 5 EGTA, and 10 HEPES, pH 7.2. The extracellular buffer was PSS, and where required, niflumic acid (100 μM) and tetraethylammonium Cl (TEA; 30 mM) were added to suppress Cl^- and K^+ currents, respectively. TEA was added to PSS by isosmotic replacement of NaCl. Current recordings were obtained with a CV201AU head stage and Axopatch 200 amplifier (Axon Instruments, Foster City, CA). Cell capacitance (C_m) was measured using 10-mV pulses from a holding potential of −70 mV with the "membrane test" feature of Clampex (Axon Instruments). Such analysis was limited to spontaneously uncoupled cells or cells uncoupled by gap junction blockers.

Fluorescence microscopy. In some experiments, membrane potential was recorded using the voltage-sensitive fluorescent probe bis(1,3-dibarbituric acid)-trimethine oxanol [$DiBAC_4(3)$; 5 μM] according to methods previously described (56). To test whether membrane potential changes are conducted from cell to cell along the DVR wall, we accessed an endothelial cell or pericyte for voltage clamp by using nystatin-perforated patches. The cell was depolarized from −70 to −30 mV while $DiBAC_4(3)$ fluorescence was monitored along the vessel wall ~200 μm away from the site of patch formation. A region of several cells was optically isolated by adjusting a rectangular window of a photon-counting photomultiplier detection assembly (D104B; Photon Technology International). $DiBAC_4(3)$ was excited at 485 nm with a DeltaRAM illuminator (Photon Technology International). Fluorescent emission at 530 nm was isolated with a bandpass filter (Omega Optical, Brattleboro, VT). Calibration of $DiBAC_4(3)$ has been described previously (27). Briefly, cellular permeability to monovalent cations was equalized by exposure to the ionophore gramicidin D (2 mg/ml). Extracellular Na^+ concentration was varied by isosmotic substitution with *N*-methyl-D-glucamine to yield 2.5, 5, 25, 50, 100, or 150 mM, and the imposed membrane potential was calculated using the Goldman equation. The associated change in $DiBAC_4(3)$ fluorescence yielded the corresponding percent change per millivolt (27, 56).

To determine whether gap junctions between cells along the DVR wall facilitate diffusion of molecules, we included the 457-Da fluorescent probe Lucifer yellow (2 mM, excitation 425 nm, emission 540 nm) in the electrode. Ruptured patches were formed on endothelial cells or pericytes, after which membrane currents were recorded to determine whether prolonged capacitance transients were present, indicating cell-to-cell coupling. Subsequently, white light and Lucifer

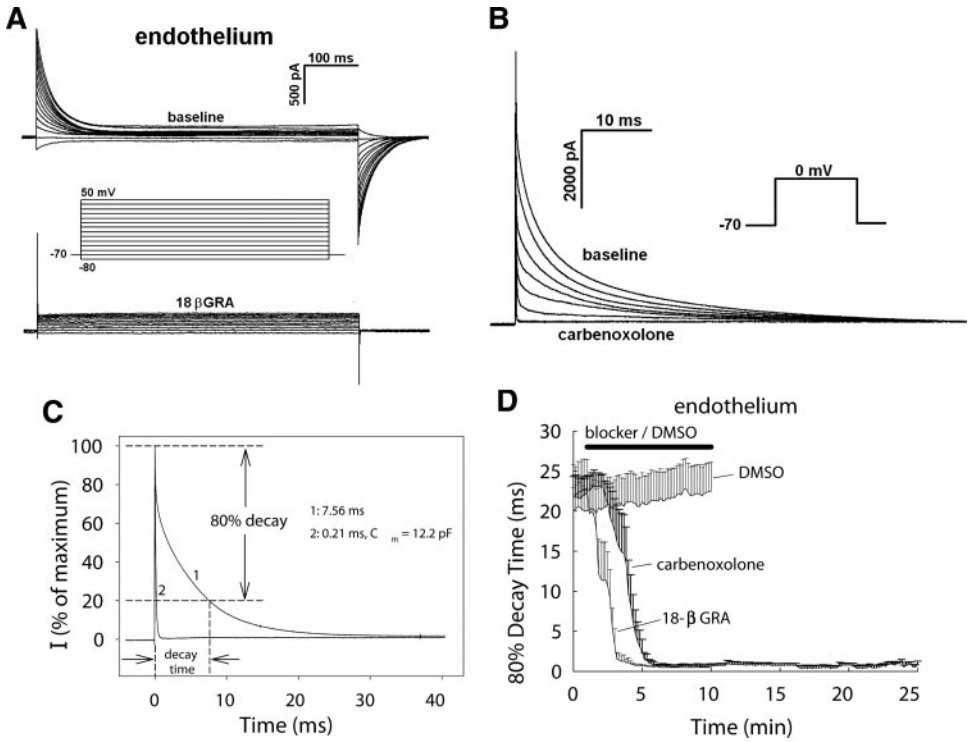

Fig. 1. Capacitance transients in descending vasa recta (DVR) endothelium. *A*: example of a whole cell current recorded from a nystatin-patched DVR endothelial cell on a pericyte-stripped vessel (44). The cell was held at −70 mV and depolarized to levels between −80 and +50 mV (10-mV increments, 500 ms). Prolonged, decaying capacitance transients, present at baseline (*top* record), were reduced to <1 ms after exposure to 18β-glycyrrhetinic acid (18βGRA; 100 μM; *bottom* record). Results are similar in $n = 5$ experiments. *B*: example of superimposed traces of capacitance transients from an endothelial cell pulsed from −70 to 0 mV at 10-s intervals. After baseline recording, the vessel was exposed to carbenoxolone (100 μM). Traces were selected from the original record to illustrate reduction of the capacitance transient decay time. *C*: method used to quantify capacitance transient decay times. *Trace 1* is the first (baseline), and *trace 2* is the last (in carbenoxolone) record from *B*. The time required for the maximum postpulse current (*I*) to fall to within 80% of baseline was 7.56 ms. After carbenoxolone, the time shortened to 0.21 ms. In the latter case, whole cell parameters permitted calculation of cell membrane capacitance (C_m = 12.2 pF). *D*: measurement of the ability of 18βGRA (100 μM, $n = 8$), carbenoxolone (100 μM, $n = 7$), and 0.1% DMSO ($n = 5$) to reduce the transient decay time of DVR endothelia. Blockers or DMSO was applied after 2 min of baseline recording. Decay time was quantified from successive pulses by using the method described in *C*. Gap junction blockers, but not DMSO, markedly reduced the decay time ($P < 0.01$ for all times >3 min for 18βGRA and times >5 min for carbenoxolone).

yellow fluorescent images were captured by timed exposure (Spot Cam; Diagnostics Instruments).

To record propagated $[Ca^{2+}]_{cyt}$ transients along the DVR wall, we loaded the Ca^{2+}-sensitive fluorescent probe fluo-4 (Molecular Probes) by incubation of the AM ester (2 μmol/l, 20 min, 37°C). The probe was excited at 485 nm (DeltaRam), and emissions were monitored at 530 nm (B-2E/C filter cube; Nikon), with a ×40 CF fluor oil-immersion objective (1.3 numerical aperture). Fluorescence was monitored by capturing sequential images, once per second, with a low light level charge-coupled device camera with on-chip multiplication gain (Photometrics Cascade 512B; Roper Scientific). A micropipette with a 10-μm orifice was positioned close to the DVR wall at one end of the vessel. At 1-min intervals, pressurization of the pipette from a reservoir was used to puff a stream of buffer onto the vessel wall. Resultant $[Ca^{2+}]_{cyt}$ transients along the vessel wall were quantified within rectangular regions of interest by using ImageMaster software (Photon Technology International).

Immunofluorescent labeling of isolated DVR. Using methods previously described (5, 33), we performed immunofluorescent labeling to detect expression of Cx37, Cx40, and Cx43 in the DVR wall. Monoclonal antibody directed against α-smooth muscle actin (SMA; 1:500 dilution to 9 μg/ml; Sigma A2547) was used to delineate the pericytes (33, 41). Rabbit polyclonal antibodies directed against Cx37 (1:50 dilution to 20 μg/ml; Alpha Diagnostic International CX37B12-A), Cx40 (1:50 dilution to 20 μg/ml; Chemicon AB1276), and Cx43 (1:100 dilution; Cell Signaling Technology 3512) were used to identify their respective distributions within pericytes and endothelium. Microdissected DVR were transferred onto slides and fixed with 3% paraformaldehyde in 100 mM cacodylate buffer, pH 7.4, and then rinsed three times. Vessels were then permeabilized with 0.1% Triton in PSS buffer for 2 min, blocked with 5% bovine serum albumin in PSS with 0.1% Triton (10 min, room temperature), and exposed to the primary antibody for 1 h at room temperature and then overnight at 4°C. After three washes with PSS containing 0.1% Triton X-100, the vessels were incubated with secondary antibodies conjugated to Alexa Fluor 488 goat anti-rabbit IgG (1:400 dilution to 5 μg/ml; Molecular Probes A-11034) and Alexa Fluor 568 goat anti-mouse IgG (1:400 dilution to 5 μg/ml; Molecular Probes A-11031) for 1 h at room temperature. After several additional washes, coverslips were mounted with Vectorshield (Vector Laboratories, Burlingame, CA). Fluorescent images were obtained using a Zeiss LSM410 scanning confocal microscope with a ×63 oil-immersion objective with a *Z*-axis 0.5-μm step size. *Z*-series overlays (SUM images) of the actin and connexin images were generated with ImageJ 1.33 (NIH) to augment the ability to localize connexins to pericytes or endothelium. Nomarski (differential interference contrast) images were obtained of the same vessel for comparison. To verify specificity, negative controls were performed in which primary antibodies were omitted.

Reagents. Lucifer yellow and $DiBAC_4(3)$ were obtained from Molecular Probes. Niflumic acid, 18β-glycyrrhetinic acid (18βGRA), carbenoxolone, heptanol, nystatin, collagenase 1A, protease XIV, and other chemicals were obtained from Sigma (St. Louis, MO). Liberase Blendzyme 1 was obtained from Roche Applied Science. Niflumic acid and 18βGRA were dissolved in DMSO. Reagents were thawed and diluted on the day of the experiment. Excess was discarded daily. Blendzyme was stored in 40-μl aliquots of 4.5 mg/ml in water and diluted into high-glucose DMEM on the day of the experiment.

Statistics. Data are reported as means ± SE. The significance of differences was evaluated with SigmaStat 3.11 (Systat Software, Point Richmond, CA) using parametric or nonparametric tests as appropriate for the data. Comparisons between two groups were performed with Student's *t*-test (paired or unpaired, as appropriate) or the rank sum test (nonparametric). Comparisons between multiple groups were performed with repeated-measures ANOVA or repeated-measures ANOVA on ranks (nonparametric). Post hoc comparisons were performed using Tukey's or Holm-Sidak tests. $P < 0.05$ was used to reject the null hypothesis. Curve fits to data points were performed using the Levenberg-Marquardt algorithm in Clampfit 9.2 (Axon Instruments).

RESULTS

Gap junction coupling in DVR endothelia. Access to DVR endothelia was achieved by removing pericytes with a micropipette (44). Endothelial whole cell currents, measured with nystatin-perforated patches, always showed large, decaying transients at the beginning of depolarizing or hyperpolarizing pulses (Fig. 1*A*). We tested whether those transients are due to the large membrane area resulting from cell-to-cell coupling through gap junctions. As shown in Fig. 1*A*, exposure to the gap junction blocker 18βGRA (100 μM) markedly shortened the transients. To quantify the effect, the transients were recorded by imposing sequential depolarizing pulses from −70 to 0 mV (100-ms duration) at 10-s intervals. During pulsation, the cells were exposed to the gap junction blockers 18βGRA (100 μM) or carbenoxolone (100 μM) or to vehicle (0.1% DMSO). An example is shown in Fig. 1*B* where sequential transients are superimposed that include baseline and subsequent traces following introduction of carbenoxolone. The marked shortening of the capacitance transients in carbenoxolone favors the interpretation that cell-to-cell coupling predominates in DVR endothelium and is eliminated by gap junction blockade.

In an isolated cell, a fit to the appropriate single-exponential relationship can yield a proper measure of cell membrane

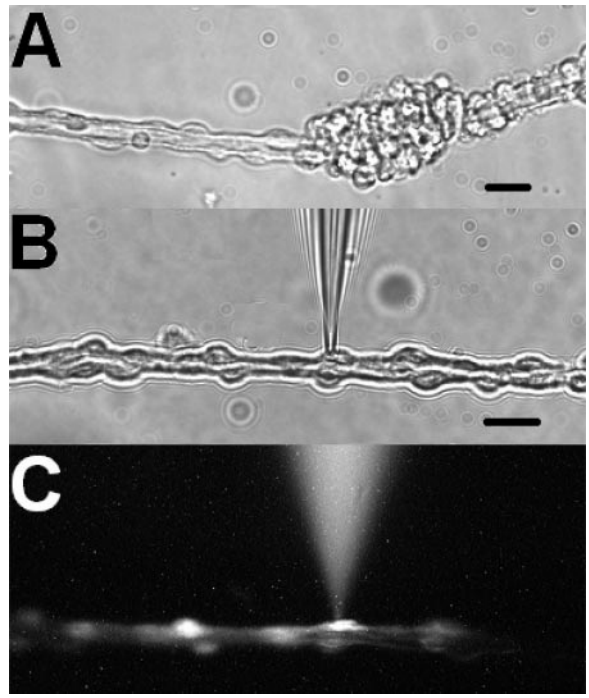

Fig. 2. Spreading of Lucifer yellow along DVR endothelia. *A*: example of a vessel in which abluminal pericytes have been partially stripped by drawing the vessel into a micropipette and ejecting it. The ball of stripped pericytes (*right* of *center*) removed from the vessel wall exposes the endothelial monolayer for patch clamp (*left* of *center*). This method has been described in detail previously (44). *B* and *C*: corresponding white light (*B*) and fluorescent images (*C*) of an endothelial layer in which the cytoplasm of 1 cell has been accessed with a ruptured patch. The patch pipette contained Lucifer yellow (457 Da, 2 mM), which diffuses throughout the cytoplasm of adjacent endothelia. Bars, 10 μm.

capacitance. In contrast, the circuit theory underlying that analysis is inappropriate for calculation of capacitance in gap junction-coupled cells (32, 35). For that reason, we chose to quantify the time course of changes in capacitance transients using the simple method illustrated in Fig. 1*C*. Custom software was written to determine the time required for membrane current to fall from the maximum that occurs at the beginning of an applied voltage pulse to within 80% of its end-pulse value. A typical application is illustrated in Fig. 1*C* where only the transients present before (*curve 1*) and long after exposure to carbenoxolone (*curve 2*) are shown. The corresponding 80% decay time falls from 7.56 to 0.21 ms. In the case of *curve 2*, it is appropriate to fit the data to a single exponential to calculate single-cell capacitance (C_m); that yields a value of C_m = 12.2 pF. Using that approach, we quantified the effects of 18βGRA, carbenoxolone, and vehicle (DMSO). Exposure to the gap junction blockers rapidly reduced the decay time of the transients (Fig. 1*D*). Neither blocker easily reversed upon washout. Sequential pulses in DMSO did not reduce decay time, verifying that 18βGRA and carbenoxolone, and not the repeated depolarizing pulses, closed the endothelial gap junctions.

Spread of Lucifer yellow along the endothelial syncytium. To obtain further evidence that endothelial cells of DVR are coupled by gap junctions, we formed ruptured patches and included the fluorescent probe Lucifer yellow (457 Da, 2 mM) in the electrode buffer. In such experiments, Lucifer yellow consistently spread between endothelial cells. Examples of white light and fluorescent images, similar to n = 8 vessels, is provided in Fig. 2.

Gap junction coupling in DVR pericytes. As previously described (5, 55), some DVR pericytes show prolonged capacitance transients that indicate gap junction coupling. Many pericytes, however, do not. Examples of current records are provided in Fig. 3. Figure 3*A*, *a* and *b*, shows whole cell records composed of submillisecond capacitance transients followed by activating currents (pulse protocol defined in *inset*). We have previously shown that the activating currents are largely carried by Cl^- influx through Ca^{2+}-activated Cl^- channels (37, 56, 59). Figure 3*B*, *a* and *b*, shows examples of pericyte whole cell records, elicited with the same pulse protocol, in which large-capacitance transients precede the activating currents. To demonstrate that the prolonged transients of such cells are due to gap junction coupling, we sequentially pulsed the pericytes from −70 to 0 mV during introduction of carbenoxolone (100 μM) into the extracellular buffer. As with endothelial cells (Fig. 1, *B* and *D*), the decay time of the pericyte transients was reduced to submillisecond time scales typical of single-cell recordings (Fig. 3C, *a* and *b*). As in the endothelium, the effects of carbenoxolone in pericytes were not readily reversible.

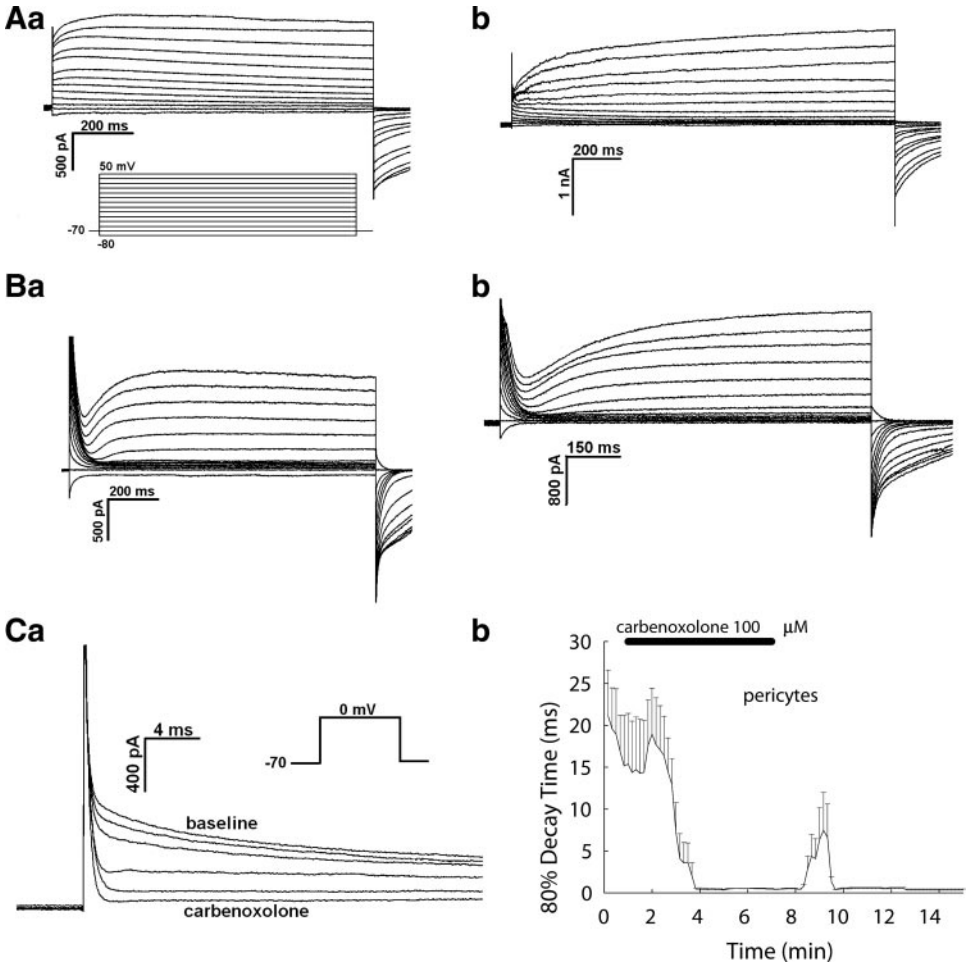

Fig. 3. Capacitance transients of whole cell records from DVR pericytes. *A*, *a* and *b*: *a* and *b* show 2 examples of DVR pericytes, accessed for whole cell recording using nystatin patches, in which capacitance transients are <1 ms. The pericytes were depolarized by the pulse protocol shown in the *inset*. *B*, *a* and *b*: *a* and *b* show 2 examples of DVR pericytes, accessed for whole cell recording using nystatin patches, in which prolonged capacitance transients indicate gap junction coupling. *Ca*: example of superimposed traces of capacitance transients from a pericyte pulsed from −70 to 0 mV at 10-s intervals. After baseline recording, the vessel was exposed to carbenoxolone (100 μM). Traces were selected from the original record to illustrate reduction of capacitance transient decay time. *Cb*: measurement of the ability of carbenoxolone (100 μM) to reduce the transient decay time of DVR pericytes. Carbenoxolone was applied after 1 min of baseline recording (n = 5). Decay time was quantified from successive pulses by using the method illustrated in Fig. 1*C*.

In a separate series, we examined the effectiveness and reversibility of 1-heptanol as a blocker of pericyte gap junctions. As shown in Fig. 4, *A* and *B*, heptanol (2 mM) was very effective; however, it also globally reduced membrane currents, implying nonspecific inhibition of membrane conductance. Unlike 18βGRA and carbenoxolone, the effects of heptanol were readily reversible upon washout. The concentration dependence of heptanol is defined by the experiment shown in Fig. 4*C* and summarized in Fig. 4*D*. At concentrations below 2 mM, inhibition of the gap junction-associated transients was incomplete.

Spread of Lucifer yellow from DVR pericytes. The data shown in Figs. 1–4 are consistent with the interpretation that the endothelium of isolated DVR is always coupled as an electrical syncytium. In contrast, cell-to-cell coupling of pericytes via open gap junctions is inconsistent. Examination of the pattern of spreading of Lucifer yellow from patched pericytes reinforced that notion. Figure 5 shows three examples of pericytes in which currents (*top*) elicited with the protocol illustrated in Fig. 4*A*, *inset*, have capacitance transients whose durations are much less than 1 ms. Corresponding white light and fluorescent images show that Lucifer yellow was confined to the patched cell. In contrast, Fig. 6 shows three examples of pericytes whose current tracings revealed prolonged transients consistent with gap junction coupling. Figure 6*A* shows a thin rim of Lucifer yellow (white arrowheads), a pattern that is expected for diffusion from cell to cell along the thin abluminal pericyte layer. Figure 6, *B* and *C*, shows examples of Lucifer yellow spread that includes transport to the endothelium. The images in Fig. 6, *B* and *C*, imply the existence of open myoendothelial gap junctions. Of a total of 27 consecutive pericytes examined by patch clamp and Lucifer yellow imaging, 8 (~30%) showed evidence of coupling, whereas 19 had only brief capacitance transients without evident spreading of the dye.

Spread of voltage clamp-induced depolarizations. To further assess the nature of cell-to-cell coupling, we tested whether depolarization of an individual pericyte or endothelial cell by voltage clamp also depolarized adjacent cells along the DVR wall. The method used for the experiment is illustrated in Fig. 7*A*. With the use of nystatin-perforated patches, an endothelial cell or pericyte was accessed for voltage clamp. The vessel was loaded with the voltage-sensitive fluorescent probe $DiBAC_4(3)$, the fluorescence of which, emitted from cells ~200 μm away from the patch pipette, was measured with a photon-counting photomultiplier detection assembly. As shown in Fig. 7*B* and summarized in Fig. 7*C*, depolarization of endothelial cells from −70 to −30 mV consistently and reversibly increased $DiBAC_4(3)$ fluorescence, verifying simultaneous depolarization of nearby cells on the DVR wall. The cells within the optical window of the photomultiplier assembly that emitted $DiBAC_4(3)$ fluorescence included both pericytes and endothelium. We cannot quantify the relative origins of the signal from the two cell types. The mean increase in fluorescence achieved by the 40-mV depolarization was 9.8 ± 2%, from which a change of 26.1 ± 5.5 mV (n = 11) was computed by $DiBAC_4(3)$ calibration. Given that some signal may have been from pericytes that did not respond, the membrane potential change in the endothelium might have been >26.1 mV. Pre-

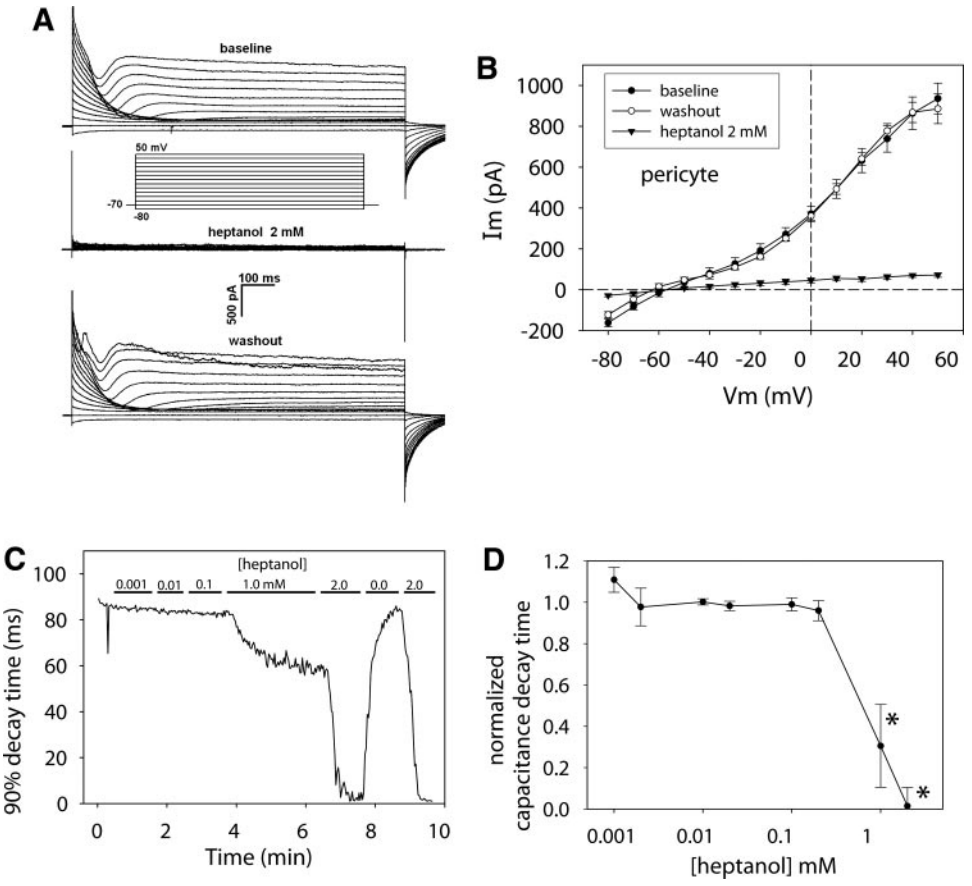

Fig. 4. Gap junction blockade of DVR pericytes by heptanol. *A*: example of whole cell current recordings from DVR pericytes at baseline (*top*), during exposure to 1-heptanol (2 mM; *middle*) and after washout (*bottom*). *B*: summary of end-pulse currents (I_m) of cells studied in *A*. Plot shows currents before (n = 10), during (n = 9), and after heptanol washout (n = 7). Heptanol was reversible, but it also reduced end-pulse currents, suggesting inhibition of overall membrane conductance. V_m, membrane potential. *C*: example of an experiment in which the concentration dependence of the ability of heptanol to reduce capacitance transients was measured. A DVR pericyte was pulsed from −70 to 0 mV, and the 90% decay time of the capacitance transient quantified as extracellular heptanol concentration was sequentially increased between 0 and 2 mM. *D*: summary of experiments similar to that in *C* (n = 2–6 cells at each concentration). *$P <$ 0.05 vs. heptanol at 0 mM. Values on the ordinate were normalized by dividing by the mean decay time at baseline, and the abscissa is presented as a log scale.

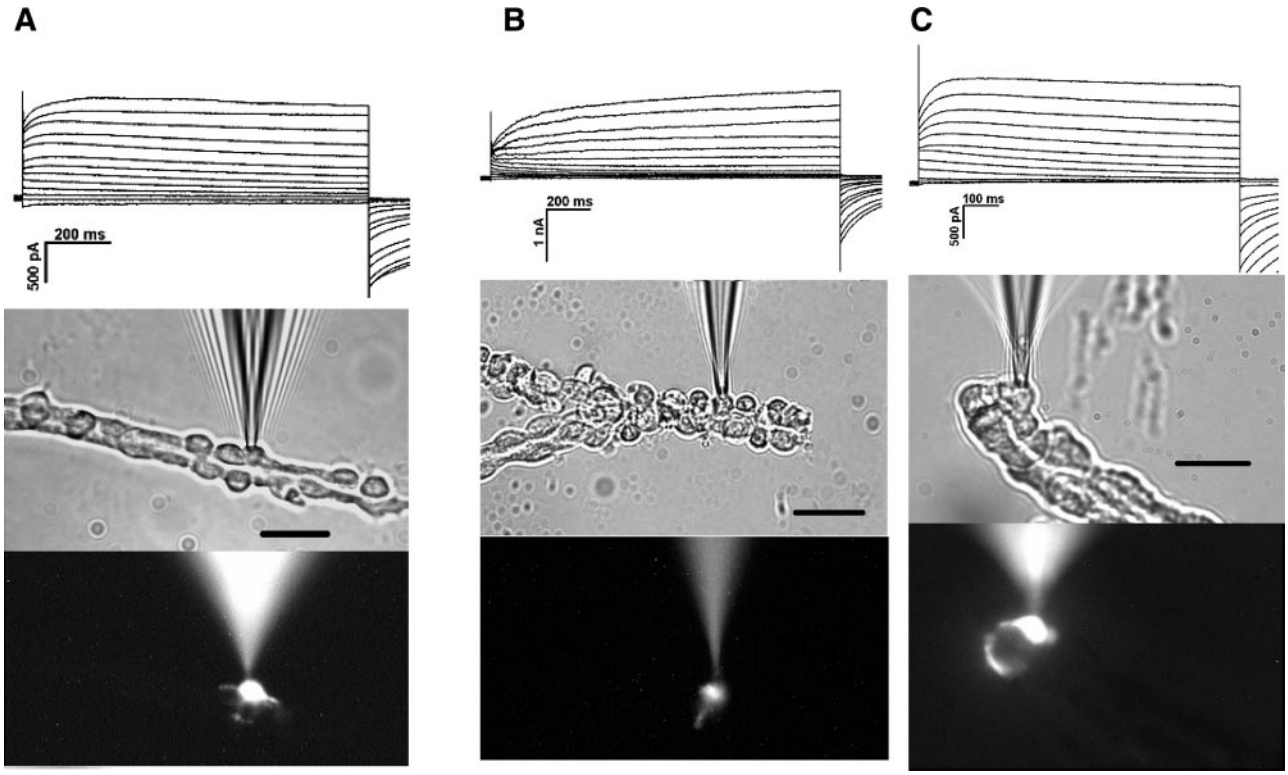

Fig. 5. Lucifer yellow spreading in pericytes with brief capacitance transients. *A–C*: 3 examples in which ruptured patches were formed on DVR pericytes by using K-aspartate electrode buffer containing Lucifer yellow. Depolarization of these cells showed capacitance transients that were <1 ms (*top*). Corresponding white light (*middle*) and fluorescent images (*bottom*) show that Lucifer yellow was confined to 1 cell (*middle* and *bottom*).

treatment with 18βGRA eliminated the change in $DiBAC_4(3)$ fluorescence that occurred upon depolarization of an endothelial cell. In contrast to the spread of depolarization from endothelia, identical depolarization of pericytes failed to alter $DiBAC_4(3)$ fluorescence (Fig. 7*D*). Those data, coupled with the results shown in Figs. 1–6, support the interpretation that the DVR endothelium is an electrical syncytium, whereas gap junction coupling in pericytes is inconsistent.

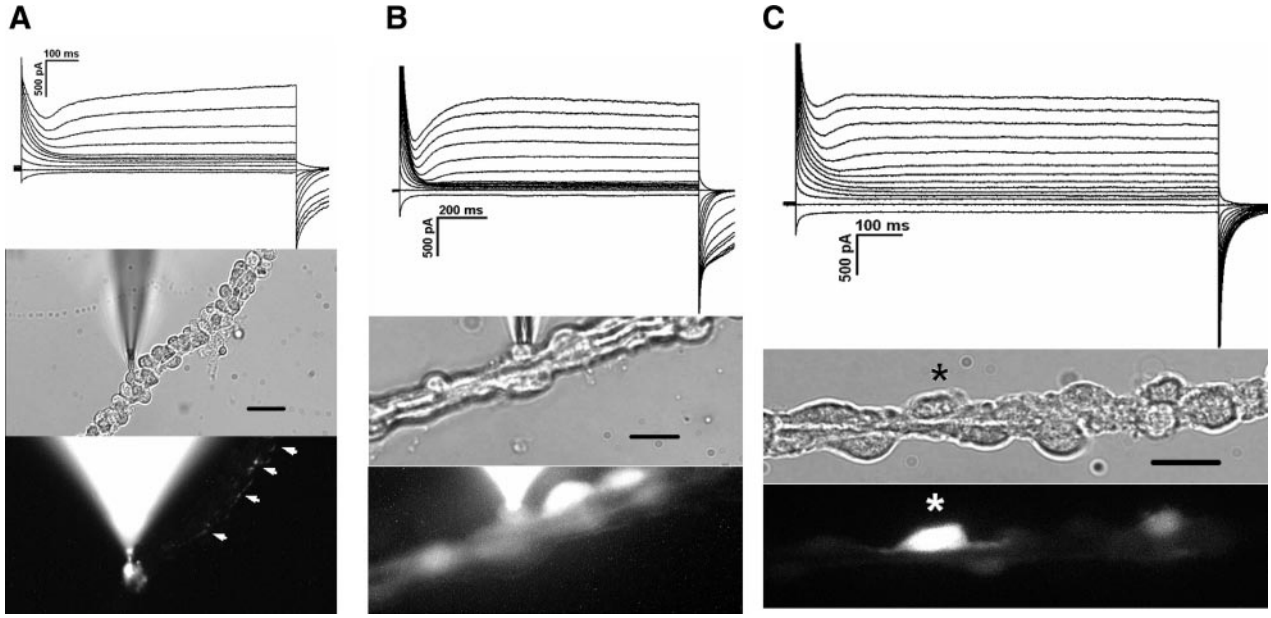

Fig. 6. Lucifer yellow spreading in pericytes with prolonged capacitance transients. *A–C*: 3 examples in which ruptured patches were formed on DVR pericytes by using K-aspartate electrode buffer containing Lucifer yellow. Depolarization of these cells showed prolonged capacitance transients (*top*), indicating gap junction coupling. Corresponding white light (*middle*) and fluorescent images (*bottom*) show variations in the pattern of spreading of Lucifer yellow. In *A*, spreading of Lucifer yellow from the patched pericyte occurs along a thin abluminal rim, indicating confinement to adjacent pericytes. In *B* and *C*, spreading of Lucifer yellow is diffuse in both pericytes and endothelium. In *C*, the pipette has been withdrawn, but the patched cell is marked with an asterisk.

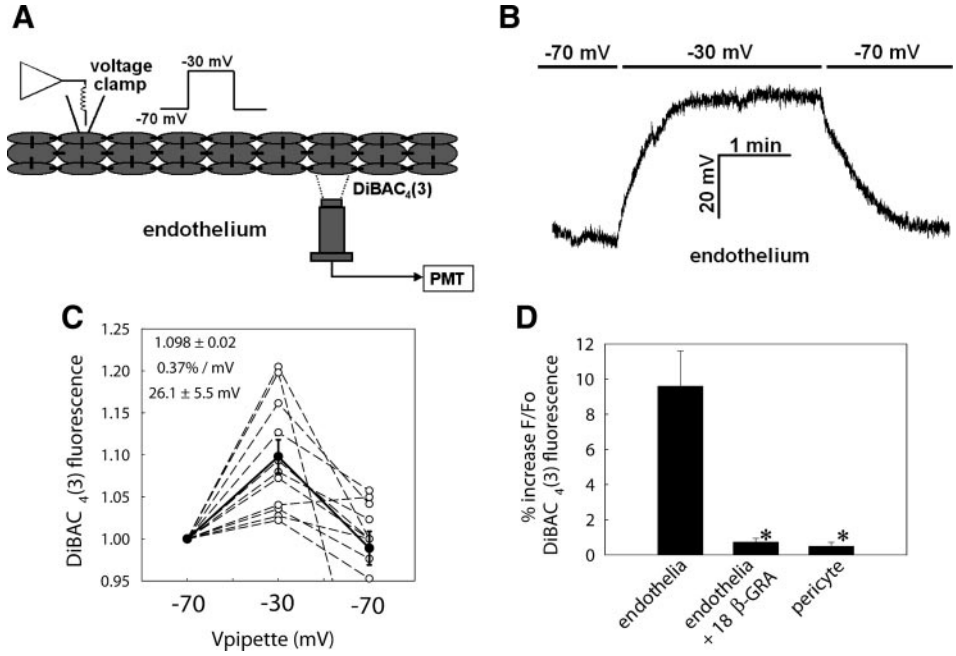

Fig. 7. Spread of depolarization between adjacent cells of the DVR wall. *A*: schematic illustration of the method used to test spread of depolarization along the DVR wall. A pericyte or endothelial cell was accessed for voltage clamp by using nystatin-perforated patches (K-aspartate electrode buffer). At the desired time point, the patched cell was depolarized from −70 to −30 mV. Bis(1,3-dibarbituric acid)-trimethine oxanol [$DiBAC_4(3)$] fluorescence was monitored in adjacent cells, ~200 μm away, using a photon-counting detection assembly. *B*: example of a record of $DiBAC_4(3)$ fluorescence during changes in the holding level of an endothelial cell from −70 to −30 mV. *C*: summary of experiments (n = 11) similar to that described in *B*. *D*: summary of %change in $DiBAC_4(3)$ fluorescence when the patch was formed on an endothelial cell, on an endothelial cell after exposure to 18βGRA, or on a pericyte without gap junction blockers (*$P < 0.01$ vs. endothelial cell alone).

Propagated $[Ca^{2+}]_{cyt}$ responses along the DVR wall. We have previously shown that the DVR endothelium is mechanosensitive. Stretch of the DVR wall by luminal pressurization induces $[Ca^{2+}]_{cyt}$ responses and NO generation (57). We exploited a variation of that property to demonstrate that $[Ca^{2+}]_{cyt}$ responses can be conducted along the DVR wall. A micropipette with an ~10-μm orifice was placed adjacent to fluo-4-loaded DVR that were adherent to the bottom of the

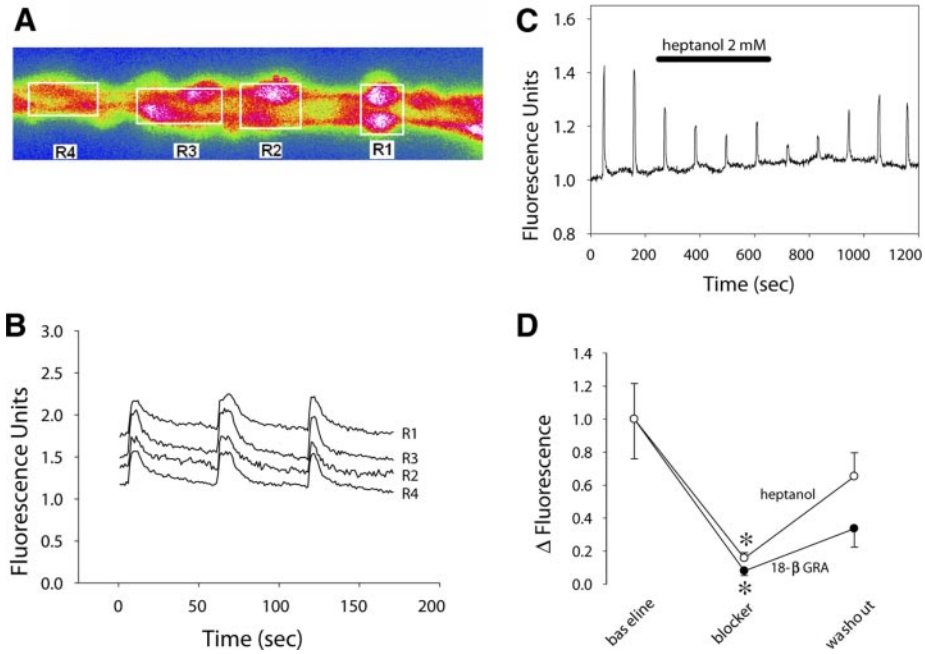

Fig. 8. Propagated cytoplasmic Ca^{2+} ($[Ca^{2+}]_{cyt}$) responses along the DVR wall. *A*: pseudocolored fluorescent image of a fluo-4-loaded DVR attached to a coverslip. Fluo-4 loaded predominantly into the endothelium. At 1-min intervals, with a micropipette, a transient stream of bathing buffer was puffed onto the abluminal surface of the vessel at one end. The pipette is not shown; it was positioned next to the left end of the vessel outside the confines of the image. A transient increase in fluo-4 fluorescence indicating a rise in $[Ca^{2+}]_{cyt}$ was observed with each puff. *B*: fluo-4 fluorescence is shown as a function of time during 4 sequential puffs. *R1–R4* correspond to the regions of interest shown in *A*. Similar $[Ca^{2+}]_{cyt}$ responses occurred all along the vessel axis. *C*: example shows reversible reduction of fluo-4 $[Ca^{2+}]_{cyt}$ responses arising from sequential puffs before, during, and after introduction of heptanol (2 mM). The region of interest for analysis was set at the most distant point from the puff pipette. *D*: summary of the fractional reduction of fluo-4 fluorescence arising from sequential puffs as in *C* upon response to heptanol (2 mM, n = 4) or 18βGRA (100 μM, n = 4). Data points show results summarized from the last puff in each period and were normalized by dividing by the mean of the peak fluorescence of the control period just before introduction of gap junction blockers. Both heptanol and 18βGRA reduced the $[Ca^{2+}]_{cyt}$ responses in a partially reversible manner (*$P < 0.05$ vs. control period).

perfusion chamber. At 1-min intervals, the pipette was briefly pressurized from a reservoir to puff a stream of buffer onto the abluminal surface of the vessel. Quantification of the fluo-4 fluorescence change within rectangular regions of interest (*R1–R4*, Fig. 8*A*) demonstrated that a $[Ca^{2+}]_{cyt}$ response was elicited at all points along the vessel axis (Fig. 8*B*). When this maneuver was performed after introduction of 18βGRA (100 μM) or heptanol (2 mM), the $[Ca^{2+}]_{cyt}$ responses were attenuated (Fig. 8, *C* and *D*). The effect of heptanol was more reversible than that of 18βGRA. As shown in Fig. 8*A*, fluo-4 distributed largely into the endothelium. These data show that endothelial $[Ca^{2+}]_{cyt}$ responses can conduct along the DVR wall in a gap junction-sensitive manner.

Immunostaining for vascular gap junction proteins. Of the connexin family proteins, Cx37, Cx40, and Cx43 are most frequently observed in the vasculature (8, 15). Double antibody immunofluorescent staining was performed in microdissected DVR to assess their presence and distribution. Counterstaining with antibody directed against SMA was used to identify pericytes (5, 33, 41). Results are shown in the reconstructions in Figs. 9–11. Antibody directed against Cx40 revealed a linear pattern largely confined to the endothelium (Fig. 9). Cx43 staining yielded a similar endothelial pattern; however, punctate staining of pericytes was more obvious (Fig. 10). Immunostaining with antibody against Cx37 yielded a pattern that was distinct from that of Cx40 and Cx43 (Fig. 11). Cx37 colocalized with SMA, implying greater expression in DVR pericytes than in endothelium.

DISCUSSION

Cell-to-cell communication through gap junctions is common in the microvasculature (4, 8, 10, 14, 15, 31, 53). It is currently understood that this occurs through transcellular channels called connexons that are formed by docking of heximeric connexin hemichannels. Connexons behave as true channels with variable open probability, subconductance states, and, in some cases, ion selectivity (3, 4). Unlike typical ion channels, however, some connexon pores are large enough to conduct diffusion of molecules as large as 1 kDa (4, 14). Homocellular connexons bridge the cytoplasm between adjacent smooth muscle cells or between adjacent endothelial cells. Heterocellular connexons, formed between smooth muscle and endothelium, yield myoendothelial gap junctions (6, 12, 17, 18, 26, 45, 50). Of some 20 connexins coded by the mammalian genome, Cx37, Cx40, Cx43, and Cx45 are found in the vasculature (14), including the microcirculation of the kidney (1, 2, 21–23, 25, 29). The functional roles of connexins are poorly understood, but cell-to-cell transfer of signaling molecules such as cAMP, inositol trisphosphate , and Ca^{2+}, as well as conduction of membrane potential changes and vasodilatory responses, have been described (11, 14, 15, 19, 20, 25).

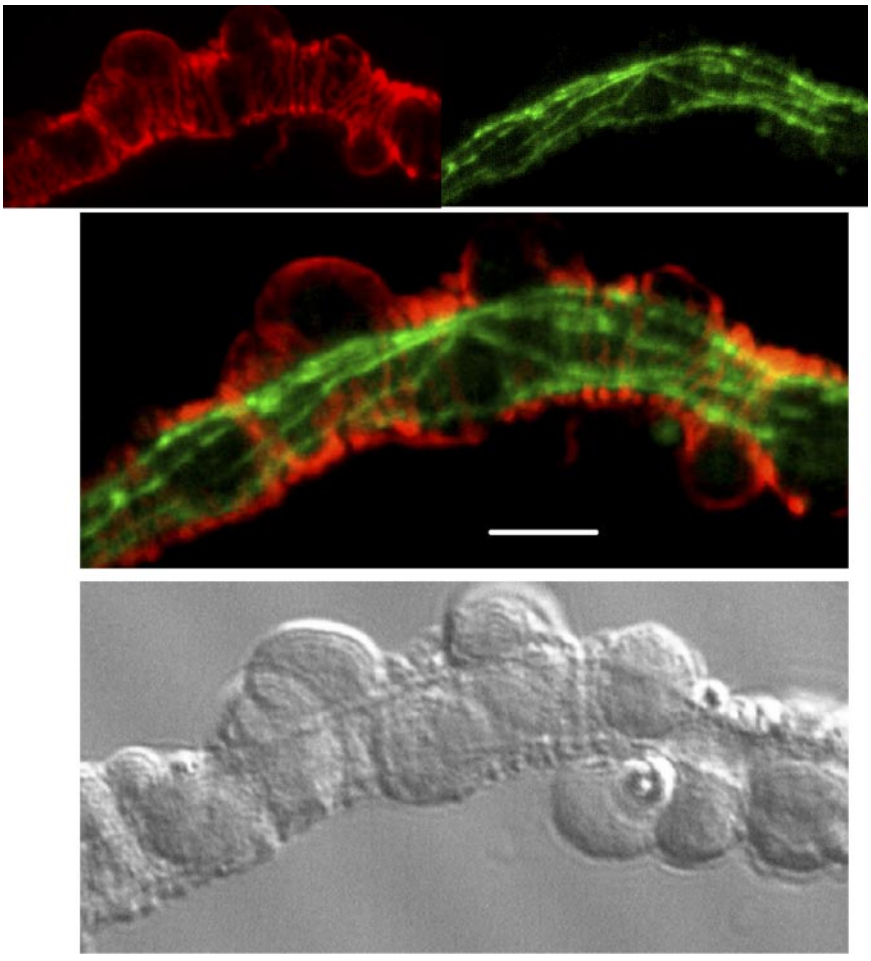

Fig. 9. Immunostaining of Cx40. Immunostaining is shown at *top* with antibody directed against α-smooth muscle actin (SMA; *left*, red) or Cx40 (*right*, green). A merged image is shown at *middle*. Bar, 10 μm. A corresponding white light image is shown at *bottom*. Cx40 showed linear staining confined to the endothelium with very little SMA colocalization. Results are similar to $n = 6$ experiments.

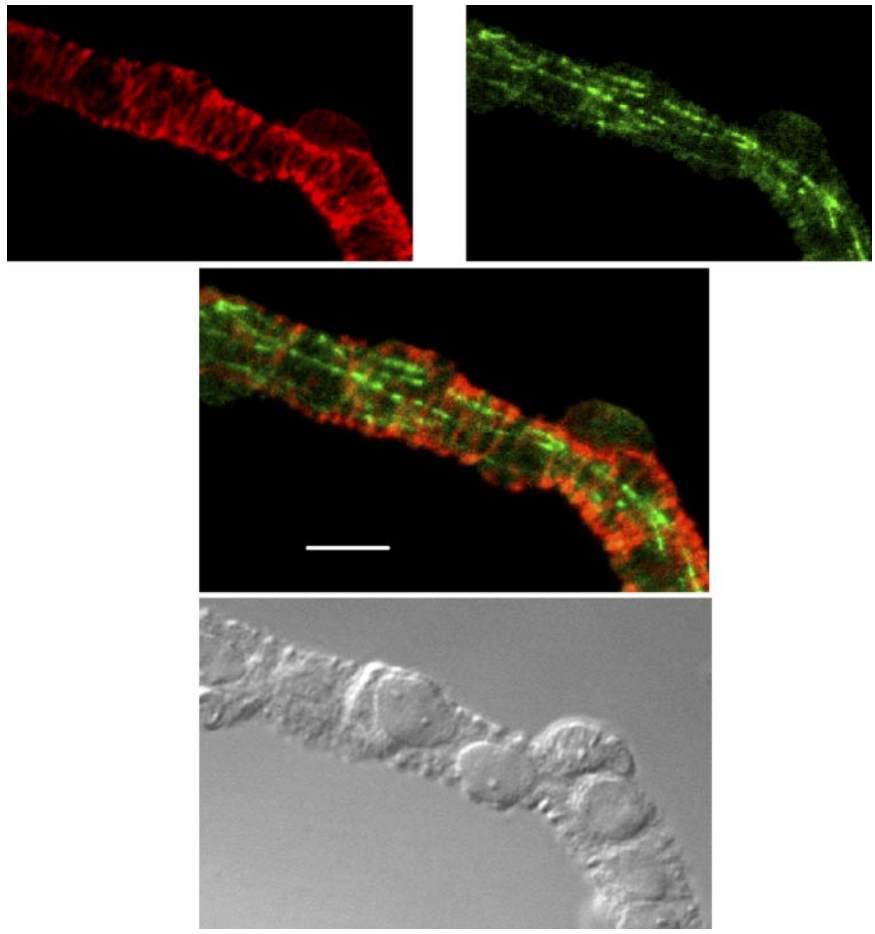

Fig. 10. Immunostaining of Cx43. Immunostaining is shown at *top* with antibody directed against SMA (*left*, red) or Cx43 (*right*, green). A merged image is shown at *middle*. Bar, 10 μm. A corresponding white light image is shown at *bottom*. Cx43 showed linear staining in the endothelium along with faint, punctate staining of pericytes. Results are similar to $n = 6$ experiments.

Myoendothelial gap junctions may be responsible for transfer of endothelium-dependent hyperpolarizing factors that limit vasoconstriction (11, 12, 17, 19, 20). Studies in transgenic mice have given some important insights into connexin function (8, 52). Because of cardiac malformation, deletion of Cx43 is lethal, implying an important role for Cx43 in morphogenesis (8, 43). $Cx43^{-/-}$ lethality is corrected when it is replaced by Cx40, but the substitution yields hypotrophic testicles and sterility (42). Separate Cx37 and Cx40 knockouts yield viable offspring except when Cx37 and Cx40 deletions are combined (47). Cx37 knockout mice lack a vascular phenotype, but deletion of Cx40 yields hypertension, irregular vasomotion, and attenuated conduction of vasodilatory responses (8, 9). Interestingly, a recent study correlated Cx40 polymorphisms with male hypertension in humans (16). In contrast to the hypertension associated with Cx40 deletion, targeted deletion of Cx43 from the endothelium using the Cre recombinase approach has been reported to reduce blood pressure (34, 49). In animal models of hypertension, expression of Cx43 has been reported to undergo variable regulation in both the peripheral and renal vasculature (24, 25), and replacement of Cx43 with Cx32 is associated with decreased renin expression and resistance to two kidney-one clip hypertension (23).

The renal medullary microcirculation is arranged as a countercurrent exchanger to accommodate the competing need to supply oxygen and nutrient blood flow while maintaining the corticomedullary gradients of NaCl and urea that enable urinary concentration. One consequence of countercurrent flow is that oxygen is shunted from DVR to ascending vasa recta so that oxygen tension in the medulla is low. A growing body of evidence favors robust release of the paracrine agents, prostaglandins, adenosine, and NO that guard against hypoxic insult by limiting microvessel constriction and by reducing Na^+ transport (7, 38, 40). Given the pivotal role of DVR in medullary perfusion, we established methods to study the channel architecture that governs their contraction and dilation (44). Cell culture models of DVR pericytes or endothelium do not exist. For that reason, we have performed electrophysiological studies on DVR explanted from the renal outer medulla by microdissection (37, 44). Isolated DVR are typically ~13 μm in diameter and 500 μm in length. Formation of gigaohm seals on abluminal pericytes has made study of their channel activity possible. In contrast, study of the endothelium has been limited by cell-to-cell coupling that is manifest during experiments by large time-decaying capacitance transients. Such large-capacitance transients are very frequent in the endothelium, implying syncytial coupling through gap junctions. In contrast, capacitance transients of pericytes are often <1 ms in duration, showing that they are uncoupled from neighboring cells (5, 55).

In this study, we verified that the prolonged capacitance transients that are always observed during patch-clamp studies of the DVR endothelium (Fig. 1), and sometimes during patch-clamp studies of DVR pericytes (Fig. 3), are a result of gap junction coupling. Several lines of investigation support

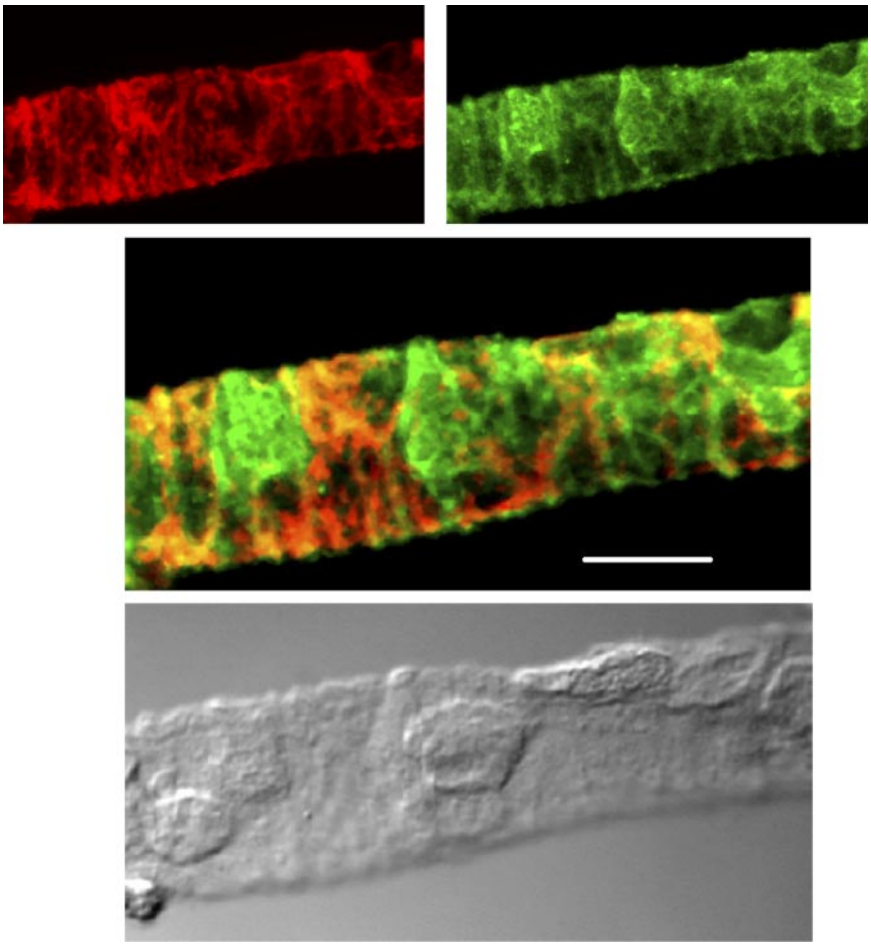

Fig. 11. Immunostaining of Cx37. Immunostaining is shown at *top* with antibody directed against SMA (*left*, red) or Cx37 (*right*, green). A merged image is shown at *middle*. Bar, 10 μm. A corresponding white light image is shown at *bottom*. Cx37 showed diffuse staining that colocalized with SMA in pericytes. Results are similar to $n = 7$ experiments.

that contention. The decay time of capacitance transients was reduced by application of the known gap junction blockers carbenoxolone, 18βGRA, and heptanol. In pericytes that exhibited prolonged capacitance transients, carbenoxolone and heptanol (Figs. 3 and 4) effectively reduced them. Dialysis of Lucifer yellow into the cytoplasm of an endothelial cell through a ruptured patch was always accompanied by diffuse spreading of the probe to neighboring cells (Fig. 2). In pericytes, the spreading patterns were complex and inconsistent. In uncoupled cells, as judged by short capacitance transients, Lucifer yellow was generally confined to a single cell (Fig. 5). In coupled cells, it sometimes diffused along the abluminal pericyte cell layer and sometimes spread to adjacent endothelium (Fig. 6). Those observations support the conclusion that although cell-to-cell coupling of pericytes is inconsistent, homocellular connexons and myoendothelial junctions do exist. Myoendothelial junctions in the kidney have been previously described (48). To examine cell coupling by an independent method, we measured the spread of a depolarizing pulse along the vessel wall. When the pulse was applied to an endothelial cell, depolarization of adjacent cells was observed and was prevented by gap junction blockade. In contrast, when the patched cell was a pericyte, depolarization did not spread along the DVR wall (Fig. 7).

Examinations of myocyte and endothelial membrane potential responses using impaled electrodes in the murine cremasteric bed, in vivo, suggested poor myoendothelial coupling (46), as we have observed. In contrast, similar studies in feed arterioles of the hamster retractor muscle showed near equivalence of membrane potential, suggesting a high degree of coupling (13). We are uncertain why DVR pericyte cell-to-cell coupling was less robust than that observed in the endothelium, but incomplete myoendothelial coupling has been reported in other microvessel preparations (15, 46). In our study, there was a substantial incidence of coupling in pericytes, but it was less uniform than that in the endothelium (Figs. 5 and 6). This may be related to the isolation of the vessels from the rat, or it may be an intrinsic property of the DVR wall. Technical limitations preclude examination of function in vivo, because the renal cortex overlies the outer medullary vascular bundles from which outer medullar DVR are derived. Warm ischemia time after harvest of the kidney from the rat and before microdissection is limited to only a few minutes, but connexins are known to be rapidly inserted and retrieved from the cell membrane. Similarly, connexins are regulated by many factors such as phosphorylation events, pH, and elevation of $[Ca^{2+}]_{cyt}$ (8, 15, 19, 24, 52). Stimulation by agonists such as endothelin and angiotensin II affects opening of gap junctions so that residual effects of those and other hormones occurring in vivo may be responsible for setting the relative open state of myoendothelial junctions (30, 31).

As with fura-2 (40), fluo-4, loaded into DVR by incubation of the esterified form, yields a predominantly endothelial signal (Fig. 8*A*). In addition, like luminal pressurization, abluminal

wall stretch induced by puffing the abluminal surface of the vessel with a localized buffer stream induces a $[Ca^{2+}]_{cyt}$ response (Fig. 8*B*) (57). The data in Fig. 8, *C* and *D*, show that the responses are attenuated by gap junction blockade with 18βGRA or heptanol. Thus gap junctions can conduct responses along the DVR wall. These data do not show whether the $[Ca^{2+}]_{cyt}$ changes are due to actual diffusion of Ca^{2+} ion between cells in Ca^{2+} waves or whether the propagation results from conduction of membrane potential changes that lead to localized Ca^{2+} signaling events. Much faster image acquisition and faster-acting fluorescent voltage-sensitive probes are likely needed to delineate and quantify those details.

To complement electrophysiological and Lucifer yellow tracer studies, we used immunochemistry with commercial antibodies to detect the presence and distribution of Cx37, Cx40, and Cx43. To aid in localization, we counterstained DVR pericytes with antibody directed against SMA. In our hands, Cx40 and Cx43 yielded a heavy, predominantly linear, staining in an endothelial pattern (Figs. 9 and 10). Lighter, punctate staining of Cx43, but not Cx40, was also observed in the pericytes (Fig. 10). The staining pattern of Cx37 was distinct from that of either Cx40 or Cx43; it was absent from endothelium, predominantly colocalizing with SMA to pericytes. Investigators have frequently reported Cx40 and Cx43 in endothelium as well as smooth muscle. In contrast, Cx37 is most often found in the endothelium (15). Thus our finding of Cx37 expression in pericytes (Fig. 11) is somewhat unusual but not unique (28, 36, 51, 54). As emphasized by Figueroa et al. (15), studies of connexin isoform distribution between endothelia and smooth muscle in both conduit arteries and microvessels have yielded diverse results. That variability may be real; to some degree, it may reflect inherent limitations of immunochemistry.

A number of studies have examined the distribution of connexins in the vasculature of the kidney. Arensbak et al. (1) observed that mRNA for Cx37, Cx40, and Cx43 is present in cultured preglomerular smooth muscle cells of the rat. In contrast, only Cx40 staining was observed by immunofluorescence or immunochemistry in tissue sections. In an extensive survey of the distribution of the same connexins in the mouse, Zhang and Hill (54) found preglomerular endothelial expression of all three isoforms at many sites between the main renal artery and the afferent arteriole. As in our study (Fig. 11), Cx37 was predominant in smooth muscle. In contrast to our findings in the rat (Fig. 10), staining of Cx37 and Cx40, but not Cx43, was observed in the murine outer medullary vascular bundles. That may be attributable to species variation, because a prior study identified robust expression of Cx43 in rat medulla and vascular bundles, similar to our observations (2, 21). Heavy Cx40 expression in juxtaglomerular cells has been described, however, with minimal expression in smooth muscle of afferent and efferent arterioles near the glomerular vascular poles (29). Modulation of renin secretion may be tied to actions of connexins in granular cells of the afferent arteriole (22, 23).

In summary, we have studied gap junction coupling of DVR pericytes and endothelium. Multiple lines of evidence lead to the conclusion that the endothelium is highly coupled by open gap junctions but that similar coupling of pericytes to one another and to the endothelial layer is inconsistent. The surreptitious nature of gap junction coupling in pericytes makes such efforts difficult to perform. It is possible that depolarizing or hyperpolarizing waves are spread between cells to regulate vasomotion in vivo. Because of the overlying renal cortex, these vessels are inaccessible, so that pertinent measurements may be difficult to obtain. If such waves do propagate along the DVR wall, an interesting, related question concerns the existence and location of a putative pacemaker, possibly in the efferent arterioles or juxtamedullary glomerulus. The possibility that the recently described voltage-operated Na^+ channels may participate in such a scheme is worthy of consideration (55). Given the ability of DVR gap junctions to conduct Lucifer yellow (457 Da), it seems reasonable to speculate that small signaling molecules such as cAMP, cGMP, Ca^{2+}, NO, and inositol trisphosphate may transfer between cells to modulate vasoconstriction and function as endothelium-dependent hyperpolarizing factors. Superoxide is generated by DVR pericytes (58) and may be conducted across myoendothelial junctions to limit bioavailability of NO. The physiological roles served by connexons in DVR require extensive studies to define.

GRANTS

These studies have been supported by National Institutes of Health Grants R37 DK-42495, R01 DK-67621, and P01 HL-78870.

REFERENCES

1. **Arensbak B, Mikkelsen HB, Gustafsson F, Christensen T, and Holstein-Rathlou NH.** Expression of connexin 37, 40, and 43 mRNA and protein in renal preglomerular arterioles. *Histochem Cell Biol* 115: 479–487, 2001.
2. **Barajas L, Liu L, and Tucker M.** Localization of connexin43 in rat kidney. *Kidney Int* 46: 621–626, 1994.
3. **Brink PR, Ramanan SV, and Christ GJ.** Human connexin 43 gap junction channel gating: evidence for mode shifts and/or heterogeneity. *Am J Physiol Cell Physiol* 271: C321–C331, 1996.
4. **Brink PR, Ricotta J, and Christ GJ.** Biophysical characteristics of gap junctions in vascular wall cells: implications for vascular biology and disease. *Braz J Med Biol Res* 33: 415–422, 2000.
5. **Cao C, Lee-Kwon W, Silldorff EP, and Pallone TL.** K_{ATP} channel conductance of descending vasa recta pericytes. *Am J Physiol Renal Physiol* 289: F1235–F1245, 2005.
6. **Chaytor AT, Edwards DH, Bakker LM, and Griffith TM.** Distinct hyperpolarizing and relaxant roles for gap junctions and endothelium-derived H_2O_2 in NO-independent relaxations of rabbit arteries. *Proc Natl Acad Sci USA* 100: 15212–15217, 2003.
7. **Cowley AW Jr, Mori T, Mattson D and Zou AP.** Role of renal NO production in the regulation of medullary blood flow. *Am J Physiol Regul Integr Comp Physiol* 284: R1355–R1369, 2003.
8. **De Wit C.** Connexins pave the way for vascular communication. *News Physiol Sci* 19: 148–153, 2004.
9. **De Wit C, Roos F, Bolz SS, Kirchhoff S, Kruger O, Willecke K, and Pohl U.** Impaired conduction of vasodilation along arterioles in connexin40-deficient mice. *Circ Res* 86: 649–655, 2000.
10. **Dhein S.** Pharmacology of gap junctions in the cardiovascular system. *Cardiovasc Res* 62: 287–298, 2004.
11. **Dora KA, Doyle MP, and Duling BR.** Elevation of intracellular calcium in smooth muscle causes endothelial cell generation of NO in arterioles. *Proc Natl Acad Sci USA* 94: 6529–6534, 1997.
12. **Dora KA, Sandow SL, Gallagher NT, Takano H, Rummery NM, Hill CE, and Garland CJ.** Myoendothelial gap junctions may provide the pathway for EDHF in mouse mesenteric artery. *J Vasc Res* 40: 480–490, 2003.
13. **Emerson GG and Segal SS.** Electrical coupling between endothelial cells and smooth muscle cells in hamster feed arteries: role in vasomotor control. *Circ Res* 87: 474–479, 2000.
14. **Evans WH and Martin PE.** Gap junctions: structure and function. *Mol Membr Biol* 19: 121–136, 2002.
15. **Figueroa XF, Isakson BE, and Duling BR.** Connexins: gaps in our knowledge of vascular function. *Physiology Bethesda* 19: 277–284, 2004.

16. **Firouzi M, Kok B, Spiering W, Busjahn A, Bezzina CR, Ruijter JM, Koeleman BP, Schipper M, Groenewegen WA, Jongsma HJ, and de Leeuw PW.** Polymorphisms in human connexin40 gene promoter are associated with increased risk of hypertension in men. *J Hypertens* 24: 325–330, 2006.
17. **Goto K, Fujii K, Kansui Y, Abe I, and Iida M.** Critical role of gap junctions in endothelium-dependent hyperpolarization in rat mesenteric arteries. *Clin Exp Pharmacol Physiol* 29: 595–602, 2002.
18. **Griffith TM, Chaytor AT, and Edwards DH.** The obligatory link: role of gap junctional communication in endothelium-dependent smooth muscle hyperpolarization. *Pharmacol Res* 49: 551–564, 2004.
19. **Griffith TM, Chaytor AT, and Edwards DH.** The obligatory link: role of gap junctional communication in endothelium-dependent smooth muscle hyperpolarization. *Pharmacol Res* 49: 551–564, 2004.
20. **Griffith TM, Chaytor AT, Taylor HJ, Giddings BD, and Edwards DH.** cAMP facilitates EDHF-type relaxations in conduit arteries by enhancing electrotonic conduction via gap junctions. *Proc Natl Acad Sci USA* 99: 6392–6397, 2002.
21. **Guo R, Liu L, and Barajas L.** RT-PCR study of the distribution of connexin 43 mRNA in the glomerulus and renal tubular segments. *Am J Physiol Regul Integr Comp Physiol* 275: R439–R447, 1998.
22. **Haefliger JA, Demotz S, Braissant O, Suter E, Waeber B, Nicod P, and Meda P.** Connexins 40 and 43 are differentially regulated within the kidneys of rats with renovascular hypertension. *Kidney Int* 60: 190–201, 2001.
23. **Haefliger JA, Krattinger N, Martin D, Pedrazzini T, Capponi A, Doring B, Plum A, Charollais A, Willecke K, and Meda P.** Connexin43-dependent mechanism modulates renin secretion and hypertension. *J Clin Invest* 116: 405–413, 2006.
24. **Haefliger JA and Meda P.** Chronic hypertension alters the expression of Cx43 in cardiovascular muscle cells. *Braz J Med Biol Res* 33: 431–438, 2000.
25. **Haefliger JA, Nicod P, and Meda P.** Contribution of connexins to the function of the vascular wall. *Cardiovasc Res* 62: 345–356, 2004.
26. **Harris D, Martin PE, Evans WH, Kendall DA, Griffith TM, and Randall MD.** Role of gap junctions in endothelium-derived hyperpolarizing factor responses and mechanisms of K^+-relaxation. *Eur J Pharmacol* 402: 119–128, 2000.
27. **He P and Curry FE.** Measurement of membrane potential of endothelial cells in single perfused microvessels. *Microvasc Res* 50: 183–198, 1995.
28. **Hill CE, Rummery N, Hickey H, and Sandow SL.** Heterogeneity in the distribution of vascular gap junctions and connexins: implications for function. *Clin Exp Pharmacol Physiol* 29: 620–625, 2002.
29. **Hwan SK and Beyer EC.** Heterogeneous localization of connexin40 in the renal vasculature. *Microvasc Res* 59: 140–148, 2000.
30. **Kawamura H, Kobayashi M, Li Q, Yamanishi S, Katsumura K, Minami M, Wu DM, and Puro DG.** Effects of angiotensin II on the pericyte-containing microvasculature of the rat retina. *J Physiol* 561: 671–683, 2004.
31. **Kawamura H, Oku H, Li Q, Sakagami K, and Puro DG.** Endothelin-induced changes in the physiology of retinal pericytes. *Invest Ophthalmol Vis Sci* 43: 882–888, 2002.
32. **Kolb HA and Somogyi R.** Biochemical and biophysical analysis of cell-to-cell channels and regulation of gap junctional permeability. *Rev Physiol Biochem Pharmacol* 118: 1–47, 1991.
33. **Lee-Kwon W, Wade JB, Zhang Z, Pallone TL, and Weinman EJ.** Expression of TRPC4 channel protein that interacts with NHERF-2 in rat descending vasa recta. *Am J Physiol Cell Physiol* 288: C942–C949, 2005.
34. **Liao Y, Day KH, Damon DN, and Duling BR.** Endothelial cell-specific knockout of connexin 43 causes hypotension and bradycardia in mice. *Proc Natl Acad Sci USA* 98: 9989–9994, 2001.
35. **Lindau M and Neher E.** Patch-clamp techniques for time-resolved capacitance measurements in single cells. *Pflügers Arch* 411: 137–146, 1988.
36. **Nakamura K, Inai T, Nakamura K, and Shibata Y.** Distribution of gap junction protein connexin 37 in smooth muscle cells of the rat trachea and pulmonary artery. *Arch Histol Cytol* 62: 27–37, 1999.
37. **Pallone TL and Huang JM.** Control of descending vasa recta pericyte membrane potential by angiotensin II. *Am J Physiol Renal Physiol* 282: F1064–F1074, 2002.
38. **Pallone TL and Silldorff EP.** Pericyte regulation of renal medullary blood flow. *Exp Nephrol* 9: 165–170, 2001.
39. **Pallone TL, Turner MR, Edwards A, and Jamison RL.** Countercurrent exchange in the renal medulla. *Am J Physiol Regul Integr Comp Physiol* 284: R1153–R1175, 2003.
40. **Pallone TL, Zhang Z, and Rhinehart K.** Physiology of the renal medullary microcirculation. *Am J Physiol Renal Physiol* 284: F253–F266, 2003.
41. **Park F, Mattson DL, Roberts LA, and Cowley AW Jr.** Evidence for the presence of smooth muscle α-actin within pericytes of the renal medulla. *Am J Physiol Regul Integr Comp Physiol* 273: R1742–R1748, 1997.
42. **Plum A, Hallas G, Magin T, Dombrowski F, Hagendorff A, Schumacher B, Wolpert C, Kim J, Lamers WH, Evert M, Meda P, Traub O, and Willecke K.** Unique and shared functions of different connexins in mice. *Curr Biol* 10: 1083–1091, 2000.
43. **Reaume AG, de Sousa PA, Kulkarni S, Langille BL, Zhu D, Davies TC, Juneja SC, Kidder GM, and Rossant J.** Cardiac malformation in neonatal mice lacking connexin43. *Science* 267: 1831–1834, 1995.
44. **Rhinehart K, Zhang Z, and Pallone TL.** Ca^{2+} signaling and membrane potential in descending vasa recta pericytes and endothelia. *Am J Physiol Renal Physiol* 283: F852–F860, 2002.
45. **Rummery NM and Hill CE.** Vascular gap junctions and implications for hypertension. *Clin Exp Pharmacol Physiol* 31: 659–667, 2004.
46. **Siegl D, Koeppen M, Wolfle SE, Pohl U, and De Wit C.** Myoendothelial coupling is not prominent in arterioles within the mouse cremaster microcirculation in vivo. *Circ Res* 97: 781–788, 2005.
47. **Simon AM and McWhorter AR.** Vascular abnormalities in mice lacking the endothelial gap junction proteins connexin37 and connexin40. *Dev Biol* 251: 206–220, 2002.
48. **Taugner R, Kirchheim H, and Forssmann WG.** Myoendothelial contacts in glomerular arterioles and in renal interlobular arteries of rat, mouse and *Tupaia belangeri*. *Cell Tissue Res* 235: 319–325, 1984.
49. **Theis M, De Wit C, Schlaeger TM, Eckardt D, Kruger O, Doring B, Risau W, Deutsch U, Pohl U, and Willecke K.** Endothelium-specific replacement of the connexin43 coding region by a lacZ reporter gene. *Genesis* 29: 1–13, 2001.
50. **Van Breemen C, Skarsgard P, Laher I, McManus B, and Wang X.** Endothelium-smooth muscle interactions in blood vessels. *Clin Exp Pharmacol Physiol* 24: 989–992, 1997.
51. **Van Kempen MJ and Jongsma HJ.** Distribution of connexin37, connexin40 and connexin43 in the aorta and coronary artery of several mammals. *Histochem Cell Biol* 112: 479–486, 1999.
52. **White TW.** Nonredundant gap junction functions. *News Physiol Sci* 18: 95–99, 2003.
53. **Yamamoto Y, Klemm MF, Edwards FR, and Suzuki H.** Intercellular electrical communication among smooth muscle and endothelial cells in guinea-pig mesenteric arterioles. *J Physiol* 535: 181–195, 2001.
54. **Zhang J and Hill CE.** Differential connexin expression in preglomerular and postglomerular vasculature: accentuation during diabetes. *Kidney Int* 68: 1171–1185, 2005.
55. **Zhang Z, Cao C, Lee-Kwon W, and Pallone TL.** Descending vasa recta pericytes express voltage operated Na^+ conductance in the rat. *J Physiol* 567: 445–457, 2005.
56. **Zhang Z, Huang JM, Turner MR, Rhinehart KL, and Pallone TL.** Role of chloride in constriction of descending vasa recta by angiotensin II. *Am J Physiol Regul Integr Comp Physiol* 280: R1878–R1886, 2001.
57. **Zhang Z and Pallone TL.** Response of descending vasa recta to luminal pressure. *Am J Physiol Renal Physiol* 287: F535–F542, 2004.
58. **Zhang Z, Rhinehart K, Kwon W, Weinman E, and Pallone TL.** ANG II signaling in vasa recta pericytes by PKC and reactive oxygen species. *Am J Physiol Heart Circ Physiol* 287: H773–H781, 2004.
59. **Zhang Z, Rhinehart K, and Pallone TL.** Membrane potential controls calcium entry into descending vasa recta pericytes. *Am J Physiol Regul Integr Comp Physiol* 283: R949–R957, 2002.